Computer Modeling in Engineering & Sciences

Tech Science Press

DOI: 10.32604/cmes.2024.055743

ARTICLE

Shear Deformation of DLC Based on Molecular Dynamics Simulation and Machine Learning

Chaofan Yao, Huanhuan Cao, Zhanyuan Xu* and Lichun Bai*

Key Laboratory of Traffic Safety on Track (Central South University), Ministry of Education, School of Traffic & Transportation Engineering, Central South University, Changsha, 410075, China

*Corresponding Authors: Zhanyuan Xu. Email: xuzhanyuan@csu.edu.cn; Lichun Bai. Email: lichunbai@csu.edu.cn

Received: 05 July 2024 Accepted: 11 September 2024 Published: 31 October 2024

ABSTRACT

Shear deformation mechanisms of diamond-like carbon (DLC) are commonly unclear since its thickness of several micrometers limits the detailed analysis of its microstructural evolution and mechanical performance, which further influences the improvement of the friction and wear performance of DLC. This study aims to investigate this issue utilizing molecular dynamics simulation and machine learning (ML) techniques. It is indicated that the changes in the mechanical properties of DLC are mainly due to the expansion and reduction of sp^3 networks, causing the stick-slip patterns in shear force. In addition, cluster analysis showed that the sp^2-sp^3 transitions arise in the stick stage, while the sp^3-sp^2 transitions occur in the slip stage. In order to analyze the mechanisms governing the bond breaking/re-formation in these transitions, the Random Forest (RF) model in ML identifies that the kinetic energies of sp^3 atoms and their velocities along the loading direction have the highest influence. This is because high kinetic energies of atoms can exacerbate the instability of the bonding state and increase the probability of bond breaking/re-formation. Finally, the RF model finds that the shear force of DLC is highly correlated to its potential energy, with less correlation to its content of sp^3 atoms. Since the changes in potential energy are caused by the variances in the content of sp^3 atoms and localized strains, potential energy is an ideal parameter to evaluate the shear deformation of DLC. The results can enhance the understanding of the shear deformation of DLC and support the improvement of its frictional and wear performance.

KEYWORDS

Diamond-like carbon; shear deformation; bond breaking/re-formation; molecular dynamics; machine learning

1 Introduction

Diamond-like carbon (DLC) films have garnered significant attention in material science due to their high hardness, similar to diamond, and good lubricity of graphite [1,2]. These films exhibit excellent properties, including high wear resistance, low coefficient of friction, and good chemical stability, which make them promising for potential applications in mechanics, electronics, optics, and biomedicine [2,3]. Meanwhile, the DLC has proven to be a key material for improving the performance and lifetime of devices, particularly in protective coatings, micromechanical devices, and energy storage devices. For instance, Wroblewski et al. [1,4,5] investigated the influence of a change in the tribological

parameters of DLC anti-wear coatings on the moment of resistance to the piston movement of an aircraft engine.

Understanding the deformation mechanisms of DLC under different conditions is essential to optimize their application procedure and predict their working lifetime and reliability. However, due to the microscale thickness of these films, it is challenging to conduct detailed analyses of their microstructural evolutions during deformation in the lab.

In recent years, molecular dynamics (MD) simulation has become a powerful tool for understanding the properties and behaviors of materials at the microscale. MD simulations can observe the structural changes of DLC during deformations at the microscale [6–8]. For example, Bai et al. [9] conducted a fatigue behavior analysis in the tensile testing of DLC films and determined that their interfacial fatigue is primarily caused by sp^3-sp^2 transition. Yu et al. [10] also conducted a uniaxial compressive simulation of DLC films and indicated that their deformation behavior results from the competition between relative slip and diffusion relaxation. However, the microstructural evolution and mechanical behaviors of DLC under shearing deformation conditions are still unclear, so their systematic deformation mechanism is still not obtained.

In order to perform more detailed simulation experiments, machine learning (ML) has been widely used in recent literature [11–13]. Deringer et al. [12] presented a methodology based on an ML representation of the density-functional theory (DFT) potential energy surface, enabling materials simulations with close-to-DFT accuracy but at a much lower cost. Xiong et al. [13] proposed a coarse-grained molecular dynamics approach to modify Tersoff's potential and reduce high-throughput computational cost by 86%. Daru et al. [11] introduced an automated strategy to perform high-quality coupled cluster molecular dynamics. The strategy can systematically improve the efficiency and accuracy of complex systems. These studies prove ML can improve simulation efficiency by extracting valuable information from plenty of data [14].

This study aims to comprehensively analyze the microstructural evolution of DLC under shear deformation conditions and their mechanical properties through MD simulations combined with ML methods. Considerations are given to the factors such as shear velocity, temperature, and loading. The investigations will emphasize the changes in bonding ratio, the relationship between shear force and various physical parameters, and the bonding breaking/re-forming mechanisms. The outcomes can improve the understanding of the mechanical behaviors of DLC under shear conditions.

2 Modeling

The atomistic model for shear deformations of DLC has the dimensions of $50 \times 15 \times 80$ Å^3, as shown in Fig. 1. The model was divided into three layers along the z-direction. The layers on both boundaries were defined as rigid bodies to avoid deformation. The middle one was regarded as a thermostatic layer in which atoms can move based on the forces given by their surrounding neighbors. During the shear simulation, the lower rigid layer was fixed with zero velocity along all three directions, but the upper layer was applied with certain x-directional velocity and y-directional loading. In order to ensure that the shear sliding happens in the middle region of the thermostatic layer, the void defects in the middle region were created by removing the C atoms. The structure of DLC was acquired using the melting-quenching method [10]; more details are provided in the literature [9]. In the shear simulation, periodic boundary conditions were applied on the x-and y-axes, while non-periodic boundary conditions were applied on the z-axis. The timestep was set to 0.1 fs. The temperature of the thermostatic layer was controlled using the Nose-Hoover thermostat.

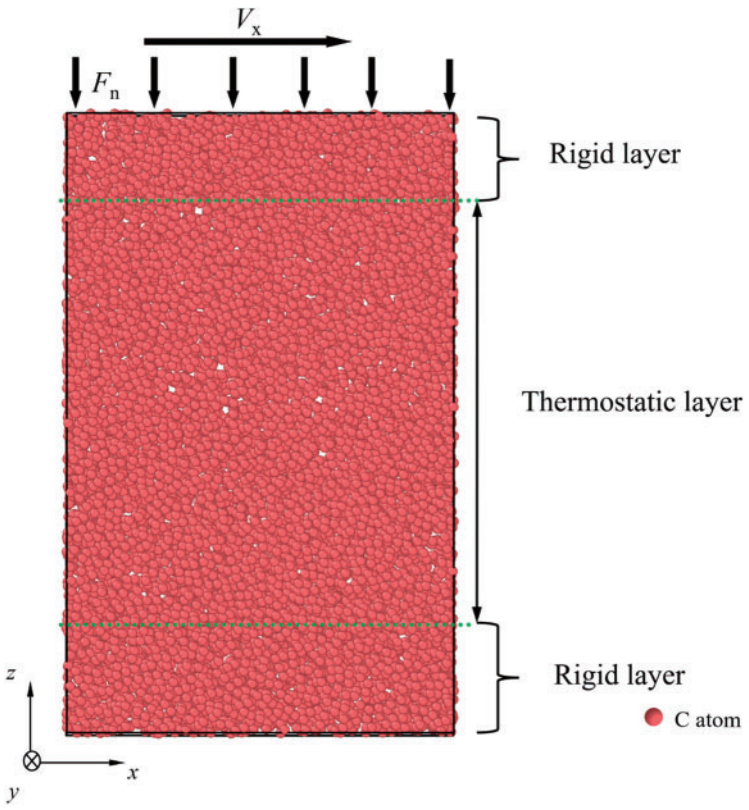

Figure 1: MD model for the shear deformation of DLC

The simulations were conducted using the open-sourced LAMMPS coding [15], and the results were visualized using OVITO software [16]. The interactions among C atoms were described using the AIREBO potential, which can accurately represent atomic interactions between C atoms [17].

The shear simulations investigated the effect of three factors, including temperature T (T = 100, 200, 300, 500, 700, 900, and 1100 K), shear velocity V_x (V_x = 0.5, 1, 1.5, and 2 Å/ps) and vertical loading F_n (F_n = 0.3, 1.2, 2.4, 3, 6, and 9 GPa). A base case was defined with T = 300 K, V_x = 0.5 Å/ps, F_n = 0.3 GPa. Only one factor was changed from the base case during the simulation, but the others were kept unchanged. The shear force F_L undertaken by DLC was calculated in the simulation by summing up all the x-directional forces of atoms in the upper rigid layer. In addition, the atomic potential energy P_e was also determined. The coordination number (C_N) of each C atom was calculated using a cut-off distance of 1.9 Å. The atoms with C_N = 3 and 4 were regarded to have sp^2 and sp^3 hybridized bonding states [18], respectively. In addition, the same cut-off distance was utilized to analyze the cluster formed by C atoms in shear deformation [10].

3 Results and Discussions

3.1 Effect of Different Factors on the Shear Performance of DLC

Fig. 2a shows the F_L *vs.* displacement (d_x) at different T. The F_L-d_x curves can be divided into three stages: elastic deformation, elastic-plastic transition, and plastic deformation. The F_L increases linearly in the first stage while showing fluctuations with stick-slip patterns in the last stage [19]. The

maximum F_L (Table 1) and the amplitude of stick-slip patterns decreases with T. The change of P_e with d_x remains consistent with that of F_L, as depicted in Fig. 2b. The initial value of P_e at the beginning of shear deformation increases with T, which seems to converse with the reported results [10]. This is because an additional F_n is applied to the DLC in the current work, which can cause the C networks to undertake compressive strain along the z-direction, which is the main difference between the current and previous models. In addition, when the DLC stays in the plastic deformation stage, the P_e decreases with the T.

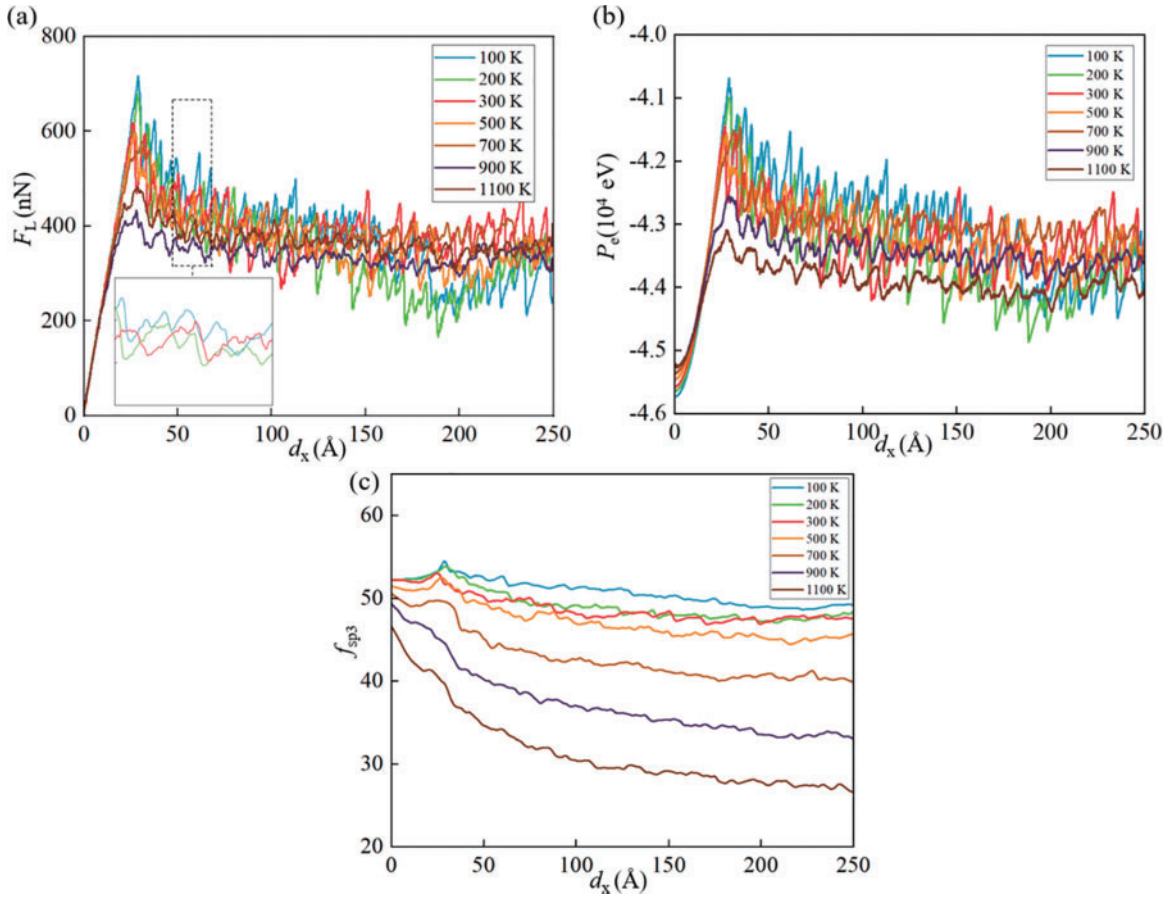

Figure 2: Dependence of (a) F_L, (b) P_e, and (c) f_{sp^3} on d_x under different temperatures

Table 1: Maximum shear force F_{max} and model height h_z along the z-direction for various temperatures

T (K)	100	200	300	500	700	900	1100
F_{max} (nN)	665.9	709.5	668.5	652.5	644.1	545.1	517.7
h_z (Å)	85.22	85.28	85.31	85.45	85.54	85.7	85.92

The changes of both F_L and P_e can be well explained by the microstructural changes of DLC that are described by the ratio of sp^3 bonding atoms f_{sp^3}, as shown in Fig. 2c. The f_{sp^3} generally decreases with the shear deformation, indicating the occurrence of graphitization of DLC, corresponding to the

decrease of F_L with d_x. In addition, a high T induces a decrease in the f_{sp^3} because the high temperature can enhance the graphitization of DLC. This is further verified by the increased height of the model along the z-direction with a high T since sp^2 atoms have a small density, and the increase of their fraction can cause the expansion of the model. The decreased f_{sp^3} also agrees well with the small F_L and P_e at a high T since the C networks with less sp^3 bonding have a low P_e and hardly undertake a high shear force. In addition, an interesting phenomenon is that the f_{sp^3} with a low T ($T < 700$ K) shows a peak in the elastic-plastic transition stage. This demonstrates that the shear strain can induce the sp^2-sp^3 transition at low temperatures, which is consistent with the observation under compressive deformation [10]. The absence of such a peak at high T can be attributed to the enhanced graphitization eliminating sp^2-sp^3 transition, corresponding to the decreased maximum F_L at a high T.

Fig. 3 illustrates the mechanical performance of DLC under various F_n. It indicates that the maximum F_L increases with the F_n. This trend is also evident in the P_e change of the DLC. In addition, the f_{sp^3} is higher under a high F_n condition than standard test conditions, as given in Fig. 3c, which can be due to the atom re-distribution induced by elastically shear deformation [20]. The above results indicate that the increase in the f_{sp^3} causes the increases in the maximum F_L and P_e, as the shear force is mainly undertaken by the network formed by the sp^3C clusters [19,21,22].

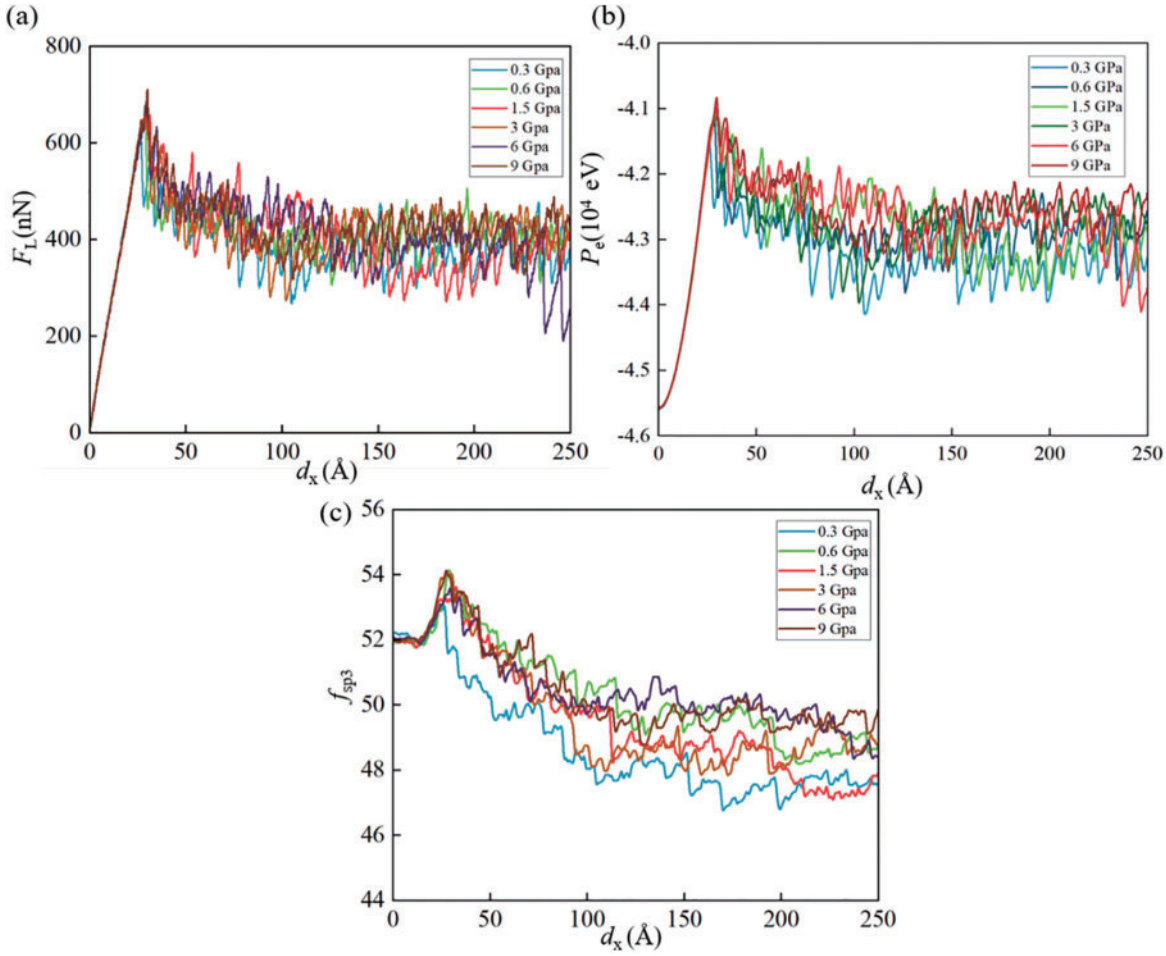

Figure 3: Dependence of (a) F_L, (b) P_e, and (c) f_{sp^3} on d_x under different loadings

Fig. 4 shows the mechanical performance of DLC under different V_x. It indicates that the DLC can withstand a larger maximum F_L and possess a higher P_e under a greater V_x condition. This can be due to the dynamic effect that occurs when higher V_x is applied externally, causing the network formed by the sp^3C-atoms to have insufficient time to rearrange atoms. In addition, the maximum f_{sp^3} present in the elastic stage slightly increases with the V_x, which is attributed to the fact that under the high deformation rate, the sp^2 atoms can become sp^3 bonding with their surrounding sp^3 networks, which also keeps consistent with the change of maximum F_L and P_e with V_x. In addition, in the plastic deformation stage, the F_L, P_e, and f_{sp^3} have little changes with the V_x, indicating that the V_x only influences the elastic deformation and has less effect on the mechanical performance of DLC than T.

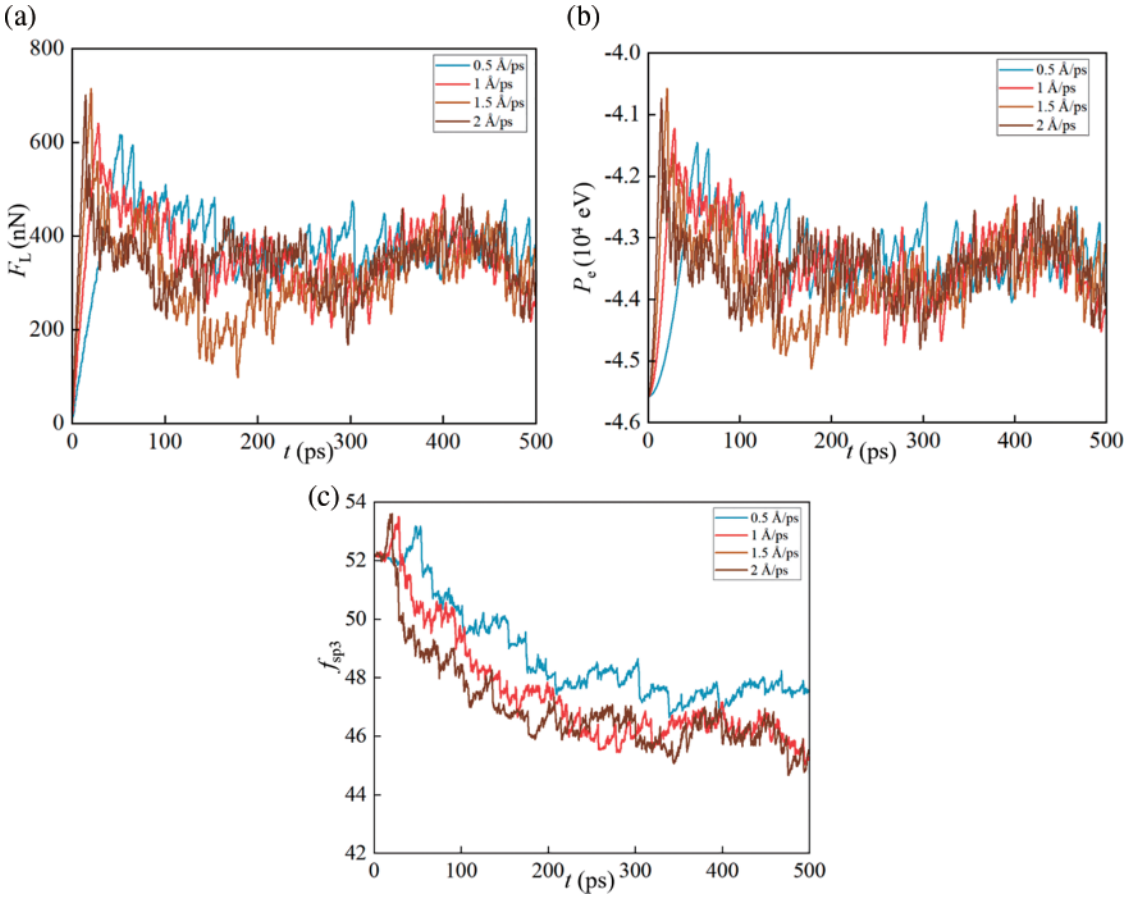

Figure 4: Dependence of (a) F_L, (b) P_e, and (c) f_{sp^3} on d_x with different shear velocities

3.2 Microstructural Evolution in the Shear Deformation

The slight increase of f_{sp^3} in the elastic stage is an exciting phenomenon governing the elastic deformation of DLC. Further analysis of the distribution of atomic force (Fig. 5a) shows that such an increase mainly happens in the middle region of the model ($40 < x < 60$ Å). The force on the C atoms increases during the elastic deformation process in such a region, which is the stick stage. However, the increased stress cannot be released due to the absence of stick-slip transitions. As a result, the sp^2 atoms near the sp^3 networks become sp^3 bonding and are merged into such networks, increasing their size until slip occurs [10]. When the stress in the localized region is beyond the mechanical strength

of DLC, the slip phenomenon happens in such region (Fig. 5b), making the sp^3 networks break and their size decrease. The stress release resulting from the slip phenomenon increases the absolute atomic velocity as atoms respond to the sudden change in stress conditions. This remains consistent with the change of cluster size distribution around the shear force wave induced by the stick-slip phenomenon, as given in Table 2. The largest s_{sp^3} is small before the shearing deformation but becomes significant when the stick occurs, decreasing in the slipping stage. Such a change pattern of f_{sp^3} is similar for every stick-slip phenomenon.

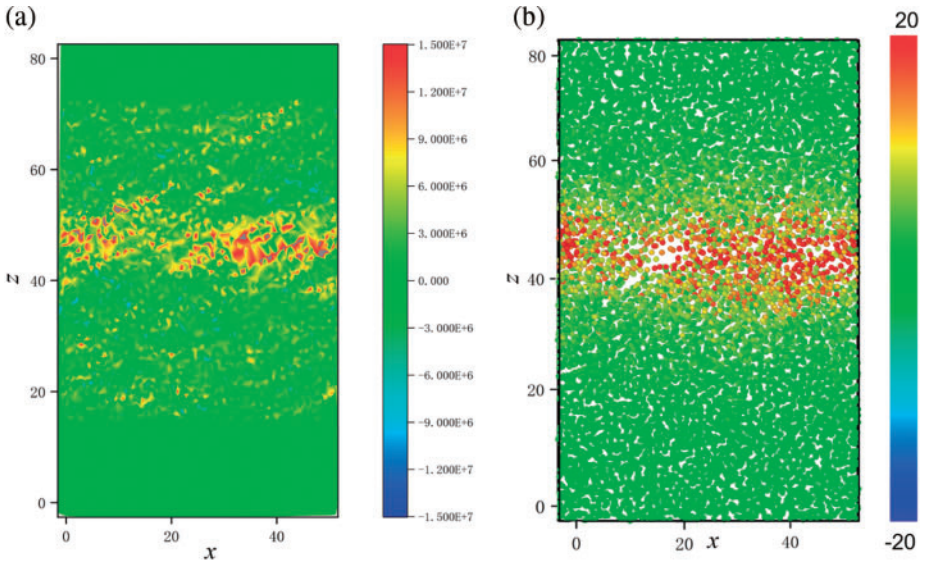

Figure 5: (a) The distribution of stress σ_{xz} in the sticking stage, and (b) the distribution of absolute atomic velocity in the slipping stage

Table 2: Evolution of the number (N_s) of sp^3 clusters with different sizes (s_{sp^3}) under 300 K. In the table, $t = 0$, 54, and 150 ps corresponds to the moment before the shearing deformation, the moment of the sticking stage, and the moment of the slipping stage, respectively

s_{sp^3}	N_s ($t = 0$ ps)	s_{sp^3}	N_s ($t = 54$ ps)	s_{sp^3}	N_s ($t = 150$ ps)
3532	1	3598	1	3295	1
4	4	4	1	28	1
3	3	3	2	10	1
2	7	2	11	8	1
1	47	1	40	5	2
/	/	/	/	4	3
/	/	/	/	3	2
/	/	/	/	2	15

The change pattern of f_{sp^3} is sensitive to different influence factors. As T increases, the sp^3 networks are easy to deform to relax the localized stress and experience the sp^3-sp^2 transition accompanied by the high T, resulting in that increasing tendency of f_{sp^3} in the elastic phase degrades gradually (Fig. 2).

For high F_n and V_x, the localization level of atomic stresses increases and promotes the increasing of the size of sp^3 networks, contributing to the higher peaks in f_{sp^3} during shearing (Figs. 3 and 4).

Since the sp^3C network is the primary carrier of the shear force in DLC, the evolution of the size of such networks induced by the bond breaking/re-formations is essential to understanding the shear deformation of DLC, which have been rarely analyzed in the previous studies [23–26]. The relation between the bond breaking/re-formations of sp^3 atoms and their surrounding environment is investigated by conducting an ML analysis. Random Forest (RF) is an ML integration method that makes predictions by constructing multiple decision trees and combining them, capable of assessing the relative importance of features [27]. In the analysis based on the RF model, the data of the properties of sp^3 atoms include their velocity, C_N, kinetic energy, P_e, and stresses in different directions. These data are divided into 70% training and 30% test sets. The RF model is trained using an RF classifier based on the training set and subsequently utilized to analyze new data verified by the test set. The model performance, including confusion matrices, Receiver Operating Characteristic (ROC) curves, and feature importance maps, are depicted in Fig. 6.

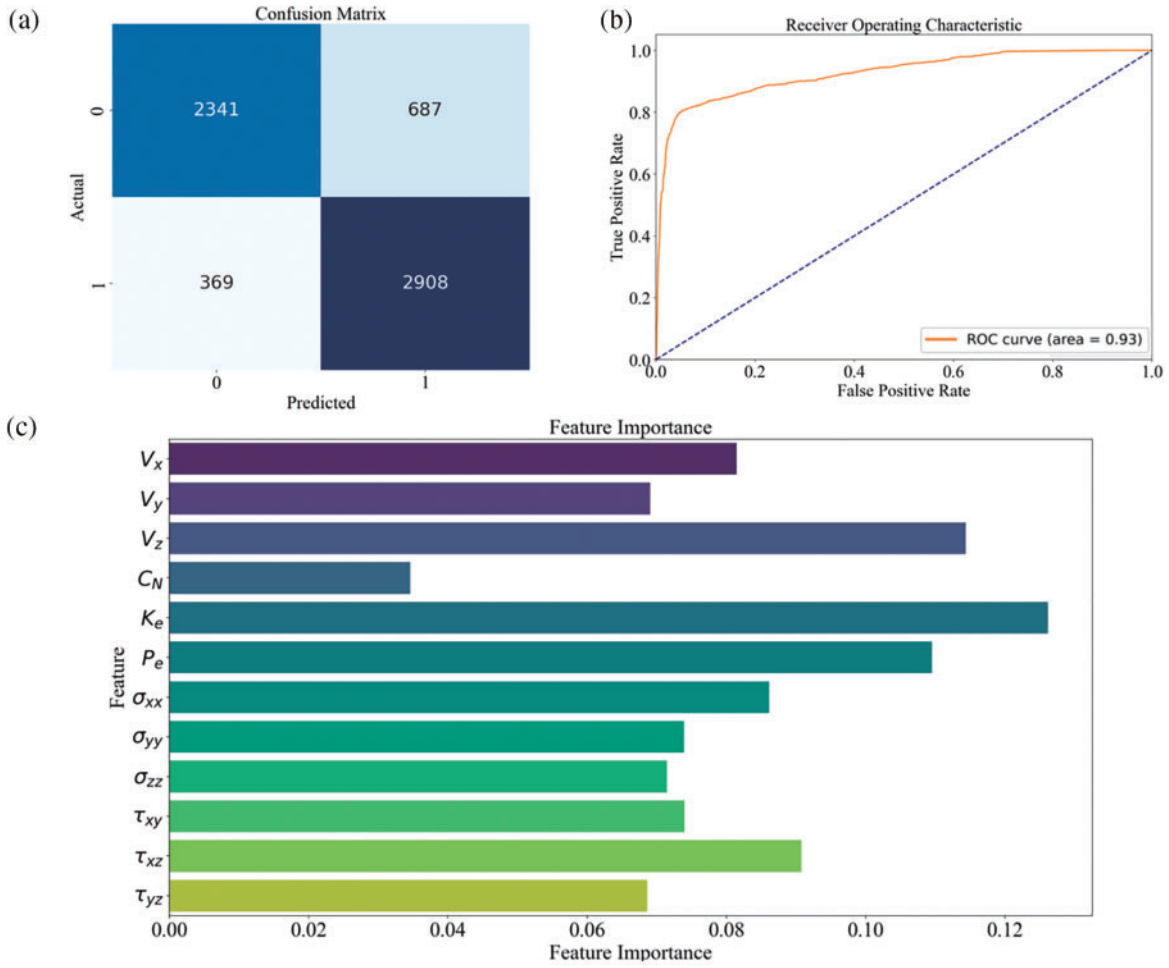

Figure 6: (a) Confusion matrix, (b) ROC matrix, and (c) eigen importance analysis obtained by the RF model for the effect of different parameters on the bond breaking/re-formation

Fig. 6a shows that 81% of the total test set consists of true and true-negative cases (i.e., correctly predicted), showing the acceptable accuracy of the trained RF model. The ROC diagram in Fig. 6b demonstrates that the model achieves an ROC Area Under the Curve (AUC) of 0.93. Since a ROC AUC close to 1 indicates the significant model balance between true and false positive cases, the current ROC AUC proves the ability of the model to classify positive and negative samples under different thresholds.

The impact of various factors on bond breaking/re-formation between sp^3 atoms can be observed through the characteristic importance plot (Fig. 6c). The kinetic energy has the maximum feature importance, indicating the greatest influence on bond breaking/re-formation. This is probably because the high kinetic energy of atoms can exacerbate the instability of the bonding state and increase the probability of bond breaking/re-formation. As the kinetic energy consists of the atomic velocities along different directions, further analysis of the impact of these velocities shows that the velocity in the z-direction (V_z) has the main contribution. This is different from the common sense that the velocity along the shear direction (x-direction in this work) dominates the changes in bonding evolution between C atoms. The influence of V_z can be attributed to the fact that the shear deformation happens in the x-z plane, and the atomic movements along the x-direction are confined due to the periodic boundary condition but have high freedom along the z-direction since the F_n applied along the z-direction is much lower than the strength of DLC and thus insufficient to confine all the atomic movement.

Regarding the influence of different types of atomic stresses, the τ_{xz} has the highest influence among them, agreeing well with the shear deformation in the x-z plane. In addition, the σ_{xx} also has a high influence, which is slightly lower than τ_{xz}. This can be due to that in the shearing regions (Fig. 5) induced by the x-z shearing deformation, the atoms entirely move along the x-direction and promote the high σ_{xx} of atoms nearby such regions, finally contributing to the bond breaking/re-formation between these atoms. In addition, P_e has a significant influence since P_e always correlates closely with the stability of the bonding state of materials, i.e., an increase in P_e caused by shear deformation and atomic movements signals a tendency for bonds to break. Hence, the impact of P_e can be regarded as a combination of the effects of stresses of atoms and the changes in their spatial positions. This is the reason why the P_e has the capability of correlating the change of f_{sp^3} in Figs. 2–4 and also in literature [6,20,28].

3.3 Relation between Shear Force and Influencing Parameters

The relation between the F_L and influencing parameters is significant to understanding the mechanical properties of DLC. The results in Section 3.1 indicate a strong relation between the F_L and f_{sp^3}. In addition, since the sp^3C networks are the primary carrier of the shear force in DLC, the factors, including the K_e (constituted by the influence of V_z) and P_e should also correlate with the F_L, due to Section 3.2, which shows that these factors have the top influence in influencing the bond breaking/re-formation between sp^3C atoms [29].

Based on the above analysis, the ML technique is employed to construct the correlation analysis for the F_L with f_{sp^3}, K_e, and P_e. The RF model, using the following parameters: 'n_estimators = 100' (number of trees), 'max_depth = None' (unlimited depth of trees), 'min_samples_split = 2' (minimum samples required to split an internal node), 'min_samples_leaf = 1' (minimum samples required to be at a leaf node), and 'random_state = 42' (ensuring reproducibility), is employed to predict F_L, as illustrated in Fig. 7. The predictions obtained from P_e in both models possess a high degree of accuracy.

However, the accuracy of the prediction from f_{sp^3} decreases, and the prediction from K_e has the worst performance.

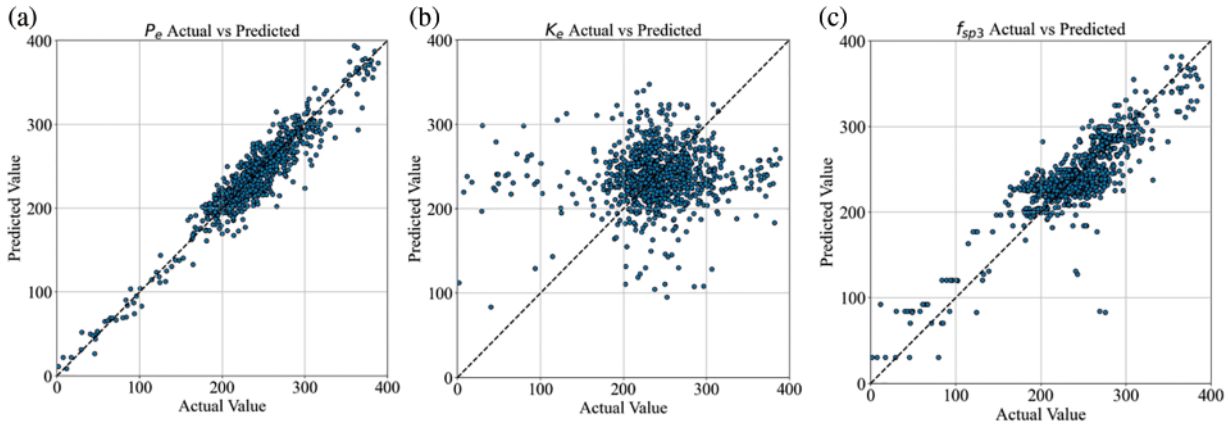

Figure 7: Relation between the actual and predicted F_L by RF model in terms of (a) P_e, (b) K_e, and (c) f_{sp^3}

The performance of the RF model is assessed by calculating the Pearson correlation coefficient, mean square error (MSE), and coefficient of determination (R^2), given in Fig. 8 and Table 3. The correlation coefficient of 0.96 and $R^2 = 0.902$ for the predictions from P_e indicate a strong positive relationship with F_L. For the predictions from f_{sp^3}, the correlation coefficient and R^2 decrease to 0.17 and 0.752, respectively, showing the decreased correlation between f_{sp^3} and F_L. These two parameters decrease further for the predictions from K_e. These results agree well with those in Fig. 7.

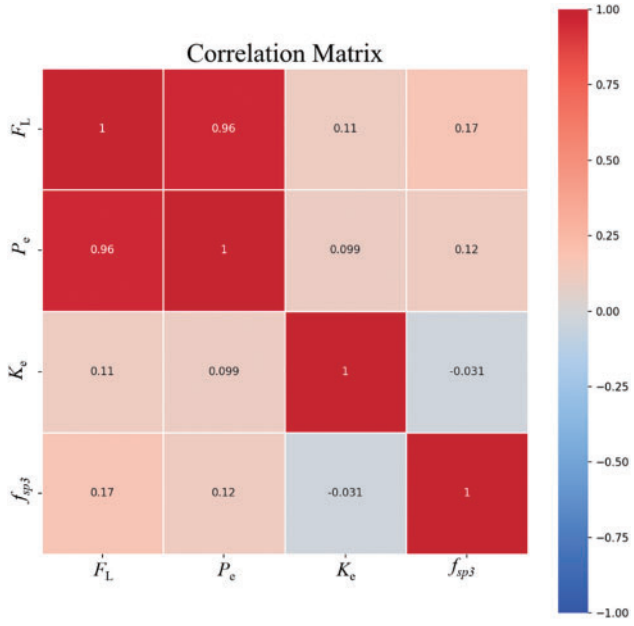

Figure 8: Correlation matrix between different parameters with F_L obtained by the RF model

Table 3: Correlation analysis and evaluation of the model

Feature	P_e	K_e	f_{sp^3}
MSE	261.398	3517.022	2562.227
R^2	0.902	−0.236	0.752

The ranking on the correlation of different parameters to F_L is quite different from the common sense of the mechanical properties of DLC. Many previous studies by both experimental and theoretical approaches have demonstrated that its deformation and easy-shear properties are dominated by the content of sp^3 and sp^2 atoms [6,30,31]. This is because the sp^3 networks are backbones in amorphous carbon structures, and the sp^2 clusters can contribute to the low shear force due to the properties of their localized π bonds, which is consistent with the observation of microstructural evolution in this study.

However, the significant influence of P_e demonstrated by the current analysis indicates that the localization strains of atoms and their bonding transition between sp^3 and sp^2 dominate the mechanical performances of DLC since the temperature (that can also affect the P_e) remains constant in this study. This exhibits that the influence of P_e includes that of f_{sp^3}. The localized contribution strains can contribute to the F_L by increasing the barrier for the mobility of atoms under shear deformation, thus improving the shear resistance of the local structure.

4 Conclusions

This study utilizes MD simulation and ML techniques to investigate the microstructural evolution and mechanical performance of DLC under shearing deformation. The findings indicated that the top ranking of different factors in terms of their influences on shear force are T, F_n, and V_x. The changes in the mechanical properties of DLC are mainly due to the expansion and reduction of sp^3 networks.

In addition, cluster analysis showed that for the stick-slip patterns observed for the shear force, the sp^2-sp^3 transitions happen in the stick stage, while the sp^3-sp^2 transitions occur in the slip stage. The RF model in ML identifies that the K_e of sp^3 atoms and their V_z has the highest influence to analyze the influence of factors on the bond breaking/re-formation in these transitions. This is because a high K_e of atoms can exacerbate the instability of the bonding state and increase the probability of bond breaking/re-formation.

Finally, the RF model finds that the F_L is highly correlated to P_e, with less correlation with f_{sp^3}. Since the changes in P_e are caused by the variances in f_{sp^3} and localized strains in this work, it is evident that P_e is an ideal parameter to evaluate the shear deformation of DLC instead of its f_{sp^3}, which is conventionally regarded as a direct parameter representing the mechanical performance of DLC. It should be noted that the MD simulations and ML models in this work are only focused on shearing conditions. The applicability of current findings on the other loading types (such as tensile and compressive deformations) should be examined in future.

Acknowledgement: The simulations in this work are supported by the High-Performance Computing Center of Central South University.

Funding Statement: The authors received no specific funding for this study.

Author Contributions: The authors confirm contribution to the paper as follows: study conception and design, Chaofan Yao; data collection, Chaofan Yao; analysis and interpretation of results, Chaofan Yao, Lichun Bai, and Huanhuan Cao; writing—original draft preparation, Chaofan Yao; writing—review and editing, Huanhuan Cao and Zhanyuan Xu; supervision, Lichun Bai and Zhanyuan Xu. All authors reviewed the results and approved the final version of the manuscript.

Availability of Data and Materials: The data that support the findings of this study are available on request from the corresponding author upon reasonable request.

Conflicts of Interest: The authors declare that they have no conflicts of interest to report regarding the present study.

References

1. Komori K, Umehara N. Effect of surface morphology of diamond-like carbon coating on friction, wear behavior and tribo-chemical reactions under engine-oil lubricated condition. Tribol Int. 2015;84:100–9. doi:10.1016/j.triboint.2014.11.010.
2. Ohgoe Y, Takada S, Hirakuri KK, Tsuchimoto K, Homma A, Miyamatsu T, et al. Investigating the functionality of diamond-like carbon films on an artificial heart diaphragm. Asaio J. 2003;49(6):701–7. doi:10.1097/01.MAT.0000093970.59796.40.
3. Fu ZQ, Sun J, Wang CB, Zhang W, Yue W, Peng ZJ, et al. Tribological performance of DLC coatings deposited by ion beam deposition under dry friction and oil lubricated conditions. Vacuum. 2013;94:14–8. doi:10.1016/j.vacuum.2013.01.006.
4. Kapsiz M, Geffroy S, Holzer A, Schmitz K. Tribological performances of diamond-like carbon coatings for hydraulic applications. Chem Eng Technol. 2023;46(1):118–27. doi:10.1002/ceat.202200459.
5. Wroblewski P, Rogolski R. Experimental analysis of the influence of the application of TiN, TiAlN, CrN and DLC1 coatings on the friction losses in an aviation internal combustion engine intended for the propulsion of ultralight aircraft. Materials. 2021;14(22):6839. doi:10.3390/ma14226839.
6. Bai LC, Srikanth N, Wu H, Liu Y, Liu B, Zhou K. Investigation on tensile behaviors of diamond-like carbon films. J Non-Cryst Solids. 2016;443:8–16. doi:10.1016/j.jnoncrysol.2016.03.025.
7. Li JH, Peng Y, Tang XQ, Xu Q, Liu B, Bai LC. Lubrication performance of hydrogenated graphene on diamond-like carbon films based on molecular dynamics simulation. Tribol Lett. 2021;69(1):1–13. doi:10.1007/s11249-020-01382-x.
8. Baimova JA. An overview of mechanical properties of diamond-like phases under tension. Nanomater. 2024;14(2):129. doi:10.3390/nano14020129.
9. Bai L, Yu Y. Fatigue behaviors of diamond-like carbon films. Diam Relat Mater. 2022;124. doi:10.1016/j.diamond.2022.108892.
10. Yu YF, Zhang X, Yin SW, Bai LC, Liu ZS. The sp^2-sp^3 transition and shear slipping dominating the compressive deformation of diamond-like carbon. J Non-Cryst Solids. 2022;577:121318. doi:10.1016/j.jnoncrysol.2021.121318.
11. Daru J, Forbert H, Behler J, Marx D. Coupled cluster molecular dynamics of condensed phase systems enabled by machine learning potentials: liquid water benchmark. Phys Rev Lett. 2022;129(22). doi:10.1103/PhysRevLett.129.226001.
12. Deringer VL, Csanyi G. Machine learning based interatomic potential for amorphous carbon. Phys Rev B. 2017;95(9). doi:10.1103/PhysRevB.95.094203.
13. Xiong Z, Yu Y, Chen H, Bai L. A coarse-grained study on mechanical behaviors of diamond-like carbon based on machine learning. Nanotechnology. 2023;34:385702. doi:10.1088/1361-6528/acde5a.

14. daFonseca BG, Thind SS, Booth I, Brolo AG. A machine learning approach for the automated classification of bulk sp^2-sp^3 carbon materials. J Raman Spectrosc. 2024;55(1):15–25. doi:10.1002/jrs.6608.
15. Humphrey W, Dalke A, Schulten K. VMD: visual molecular dynamics. J Mol Graph Model. 1996;14(1):33–8, 27–8. doi:10.1016/0263-7855(96)00018-5.
16. Stukowski A. Visualization and analysis of atomistic simulation data with OVITO-the open visualization tool. Model Simul Mater Sc. 2010;18(1). doi:10.1088/0965-0393/18/1/015012.
17. Hoehnerbach M, Bientinesi P. Accelerating AIREBO: navigating the journey from legacy to high-performance code. J Comput Chem. 2019;40(14):1471–82. doi:10.1002/jcc.25796.
18. Ma TB, Wang LF, Hu YZ, Li X, Wang H. A shear localization mechanism for lubricity of amorphous carbon materials. Sci Rep. 2014;4. doi:10.1038/srep03662.
19. Rysaeva LK, Lisovenko DS, Gorodtsov VA, Baimova JA. Stability, elastic properties and deformation behavior of graphene-based diamond-like phases. Comput Mater Sci. 2020;172. doi:10.1016/j.commatsci.2019.109355.
20. Wang JX, Wang LJ, Chen H, Wang HY. Molecular dynamics simulation of friction in DLC films with different sp^3 contents. Tribol Int. 2023;190. doi:10.1016/j.triboint.2023.109050.
21. Huang J, Peng J, Qiu X, Li X. Evolution of the microstructure, hybridization, and internal stress of Al-doped diamond-like carbon coatings: a molecular dynamics simulation. Langmuir. 2023;39(11):3895–904. doi:10.1021/acs.langmuir.2c03200.
22. Jarratt M, Stallard J, Renevier NM, Teer DG. An improved diamond-like carbon coating with exceptional wear properties. Diam Relat Mater. 2003;12(3–7):1003–7. doi:10.1016/s0925-9635(02)00296-0.
23. Baimova JA, Galiakhmetova LK, Mulyukov RR. Diamond-like structures under hydrostatic loading: atomistic simulation. Comp Mater Sci. 2021;192:110301. doi:10.1016/j.commatsci.2021.110301.
24. Muniz AR, Machado AS, Maroudas D. Mechanical behavior of interlayer-bonded nanostructures obtained from bilayer graphene. Carbon. 2015;81:663–77. doi:10.1016/j.carbon.2014.10.003.
25. Rahman SM, Song J, Yeo C-D. Computational study on surface energy of amorphous DLC with respect to hybridization state of carbon and potential functions. Diam Relat Mater. 2019;95:127–34. doi:10.1016/j.diamond.2019.04.015.
26. Shen B, Chen SL, Sun FH. Investigation on the long-duration tribological performance of bilayered diamond/diamond-like carbon films. P I Mech Eng J-J Eng. 2014;228(6):628–41. doi:10.1177/1350650114522611.
27. Breiman L. Random forests. Mach Learn. 2001;45(1):5–32. doi:10.1023/a:1010933404324.
28. Yue ZF, Wang H, Fan XQ, Li H, Zhang JY, Zhu MH. Regulating the fretting behavior of diamond-like carbon films by changing the composition and structure. Carbon. 2023;212:118097. doi:10.1016/j.carbon.2023.118097.
29. Dankesreiter B, Song JG, Rahman SM, Shah NMR, Yeo CD. Effects of diffused hydrogen atoms on thermomechanical properties and contact behavior of a diamond-like carbon film. J Appl Phys. 2021;130(2):9. doi:10.1063/5.0051339.
30. Wang LP, Bai LC, Lu ZB, Zhang GA, Wu ZG. Influence of load on the tribological behavior of a-C films: experiment and calculation coupling. Tribol Lett. 2013;52(3):469–75. doi:10.1007/s11249-013-0230-y.
31. Gershman I, Mironov A, Mezrin A, Torskaya E, Kuznetsova T, Lapitskaya V, et al. Effect of sp^3-sp^2 transformation on the wear rate of the DLC coating. Lubricants. 2022;10(5):85. doi:10.3390/lubricants10050085.